Article

Combined Strengthening Techniques to Improve the Out-of-Plane Performance of Masonry Walls

Elena Ferretti [1,*] and Giovanni Pascale [1]

[1] Department of Civil, Environmental and Materials Engineering – DICAM, Alma Mater Studiorum Università di Bologna, Viale del Risorgimento 2, 40136 Bologna, Italy; elena.ferretti2@unibo.it; giovanni.pascale@unibo.it

* Correspondence: elena.ferretti2@unibo.it; Tel.: +39-051-209-35-15

Abstract: The purpose of this study is to improve the performance of walls under out-of-plane loads, particularly when subjected to the hammering action of the floors. The idea behind the paper is to provide the masonry walls with a device that behaves like a buttress, without having to build a traditional buttress. The solution presented here consists of a mechanical coupling between the three-dimensional net of steel ribbons of the CAM system and the CFRP strips. Since the steel ribbons of the CAM system have a pre-tension, the mechanical coupling allows the steel ribbons to establish a semi-rigid transverse link between the CFRP strips bonded on two opposite sides of a wall. Therefore, two vertical CFRP strips tied by the steel ribbons behave like the flanges of an I-beam and the flexural strength of the ideal I-beam counteracts the out-of-plane displacements of the wall. The experimental results showed that the combined technique inherits the strong points of both constituent techniques: the delamination load is comparable to that of the specimens reinforced with the CFRP strips and the overall behavior is ductile as for the specimens reinforced with the CAM system. They also allowed us to design a more performing combined technique.

Keywords: Masonry buildings; Out-of-plane strength; Hammering actions; Seismic retrofitting; Bracing; Dissipative systems; CAM system; CFRP strips

1. Introduction

When the earthquake direction is orthogonal to a wall of a multi-story building, the wall receives subsequent out-of-plane thrusts from the floors, due to the oscillatory nature of the earthquake forces. In this case, we say that the floors exert a hammering action on the wall.

The subsequent pulses of the earthquake may lead the wall to either overturn or break into two parts: this second failure mechanism, the most usual one, activates when an upper kerb retains the wall and takes place with either a partial mechanism (Figure 1a) or a global mechanism (Figure 1b).

In both cases, the wall breaks with the formation of a third hinge in correspondence of one of the floors (Figure 2). As far as the meaning of symbols in Figure 2 is concerned:

- s is the thickness of the wall;
- h is the height of the wall;
- W is the self-weight of the wall;
- P_s is the weight transmitted to the wall by the floor;
- N is the weight of upper walls and floors;
- F_V is the vertical component of the thrusts given to the wall by arches and vaults;
- F_H is the horizontal component of the thrusts given to the wall by floors, arches and vaults;
- a is the distance between P_s and the hinge in B;
- d is the distance between N and the hinge in B;
- d_V is the distance between F_V and the hinge in B;

Preprints (www.preprints.org) | NOT PEER-REVIEWED | Posted: 20 February 2019 doi:10.20944/preprints201902.0194.v1

Peer-reviewed version available at Materials 2019, 12, 1171; doi:10.3390/ma12071171

- h_V is the distance between F_H and the hinge in B.

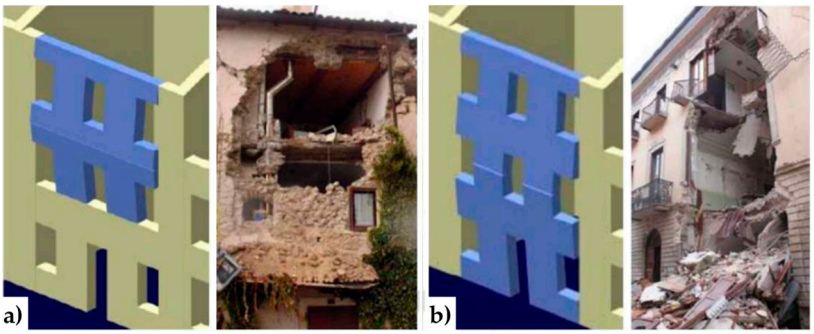

Figure 1. Out-of-plane collapses in presence of an upper kerb: a) partial collapse; b) global collapse.

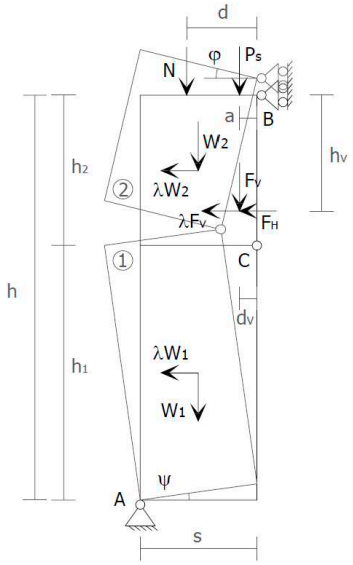

Figure 2. Failure mechanism for the hammering action of a floor when an upper kerb retains the wall: the internal hinge makes the system a labile scheme.

Avoiding the mechanisms of out-of-plane collapse that originate from the hammering action of floors is one of the main concerns in modern seismic retrofitting of masonry buildings [1–3]. Actually, engineers have been addressing the problem of counteracting the out-of-plane displacements since the dawn of building technology. One of the first architectural means used for providing support against the lateral forces is the buttress, that is, a structure built against or projecting from a wall (Figure 3): early examples of buttresses are found on the Eanna Temple (ancient Uruk), dating to as early as the 4th millennium BCE.

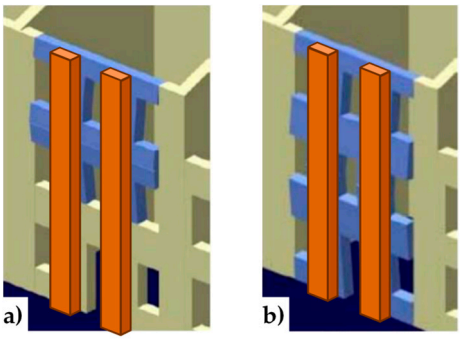

Figure 3. Principle of operation of buttresses, to prevent: a) a partial collapse; b) a global collapse.

Peer-reviewed version available at Materials 2019, 12, 1171; doi:10.3390/ma12071171

Historically, buttresses served to strengthen large walls or buildings such as churches. Nowadays, they continue to be useful in large structures such as retaining walls and dams. In these cases, and whenever buttresses counteract, or retain, the lateral force of water or earth, they may be referred to as counterforts.

To prevent the buttress projecting too much from the wall, it is possible to make the buttress in the thickness of the wall. In this second case, we must cut the wall for its entire height, build the buttress and restore the masonry wall all around it.

Both the external and embedded buttresses are effective, but highly invasive. Moreover, the external buttresses lead to increments of mass that enhance the attraction of seismic forces and the embedded buttresses often involve significant difficulties of realization.

In this paper, the authors propose to recuperate the simple idea of the buttress for out-of-plane bracing of walls in masonry buildings, but using new materials and new techniques. Our goal will be twofold: to build a minimally invasive buttress and not to increase the final weight of the retrofitted building too much. Since one of the main concerns in retrofitting masonry buildings is to guarantee a box-type behavior, we have developed the new techniques as improvements of the CAM system, a new three-dimensional continuous retrofitting system that establishes good connections between all the structural elements of the building.

2. Some basic notions of the CAM system

The CAM system consists of a three-dimensional net of stainless steel ribbons, which form closed loops passing through some holes, obtained by drilling the thickness of the masonry wall (Figure 4a). The use of stainless steel allows us to avoid corrosion problems [4]. When clamping the ribbons, a special tool provides a pre-tension to the ribbons, which then post-compress the masonry that they wrap (Figure 4b). Therefore, the CAM system is an active reinforcement technique that uses tensioned steel ribbons to strengthen the masonry in the same way as the metallic straps strengthen the packages in heavy applications. Because of this analogy, we will call the tensioned ribbons of the CAM system "the straps".

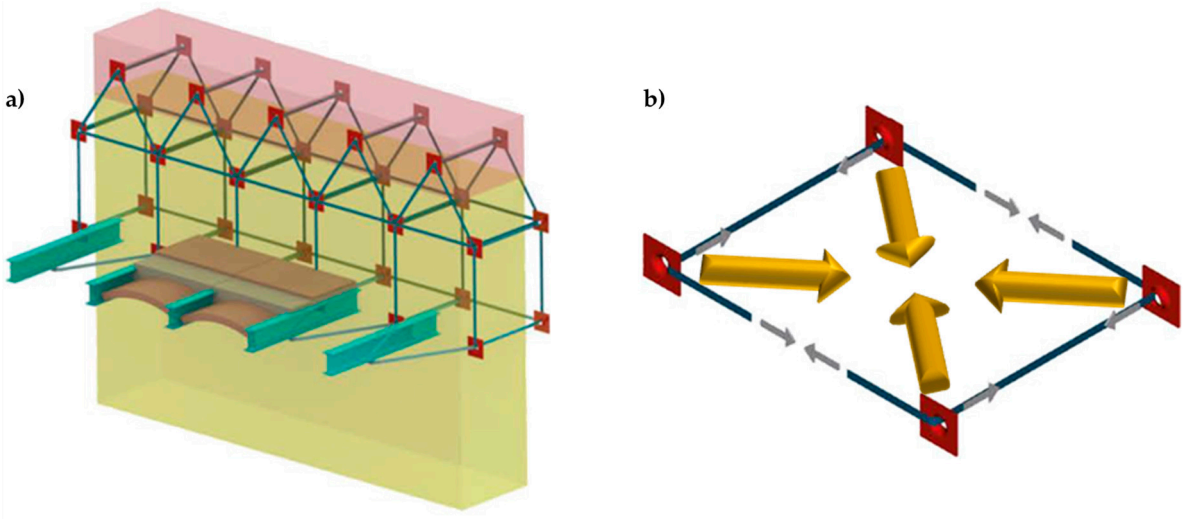

Figure 4. a) The three-dimensional net of steel ribbons of the CAM system; b) How a pre-tensioned steel ribbon compresses the masonry.

Each drilled hole serves for the passage of up to 6 straps with different directions. Therefore, the transverse holes divide the wall into units of masonry that receive a post-compression by the pre-tensioned straps. In the case of rectangular arrangement of the holes, as in Figure 4a, the units of masonry have the shape of parallelepipeds.

In [5], we have shown that the nodes of the rectangular CAM net are subjected to pairs of equal and opposite forces in the plane of the wall (Figure 5a). Consequently, they do not receive any in-

Peer-reviewed version available at Materials 2019, 12, 1171; doi:10.3390/ma12071171

plane force from the retrofitting system and do not have neither horizontal nor vertical displacements. The only nodal force not balanced by an equal and opposite force is the transverse force (Figure 5b). This means that the actual mechanism of stress-transfer from the rectangular CAM net to the masonry wall is not hydrostatic (Figure 6a), as was believed in the early studies on the CAM system [6–13]. In fact, by eliminating the balanced forces, only the transverse forces will remain, as shown in Figure 6b. Being aware of this last statement is of paramount importance for a structural engineer, as one of the main consequences of replacing Figure 6a with Figure 6b is that the value of stress in the straps becomes upper bounded. In other words, there is an upper limit value of the strap stress, which we cannot overcome without damaging the masonry [5].

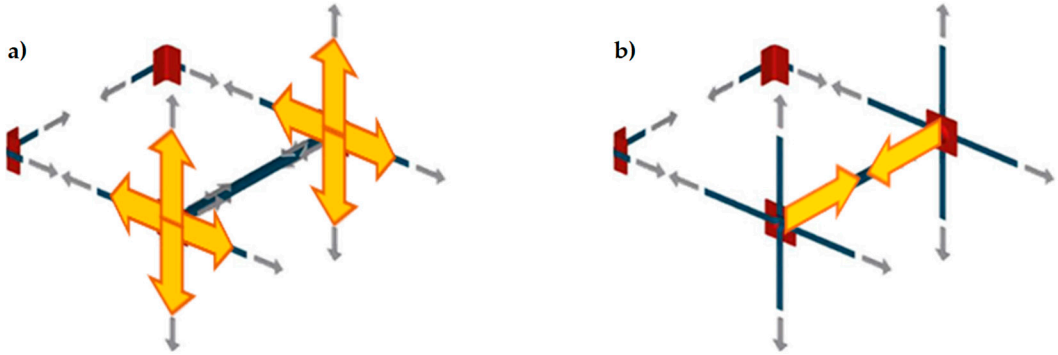

Figure 5. a) Nodal forces in the plane of the wall; b) Nodal forces in the thickness of the wall.

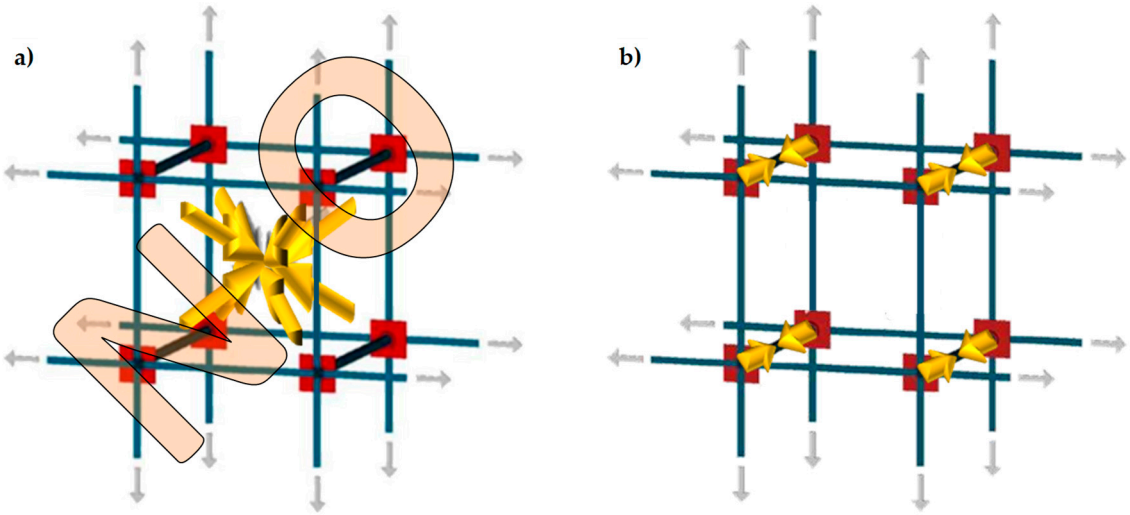

Figure 6. a) Stress transfer in the hydrostatic state of stress; b) Actual scheme of stress transfer.

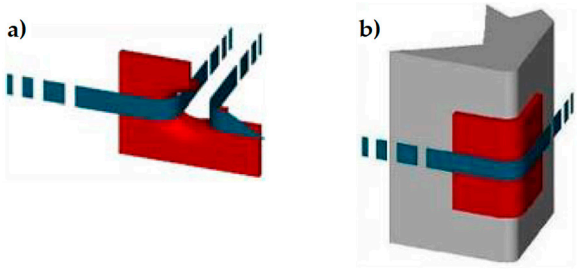

Figure 7. a) Funnel plates of the CAM system; b) Rounded angles of the CAM system.

The red elements in Figure 4-Figure 6 are stainless steel protective elements, used in the CAM system to avoid damages at the loop corners when putting in tension the straps. Their design is an

Peer-reviewed version available at Materials 2019, 12, 1171; doi:10.3390/ma12071171

integral part of the CAM patent, filed in 1999 by Dolce and Marnetto. In particular, the patent consists of funnel elements to protect the contours of the holes (Figure 7a) and rounded angles to protect the corners (Figure 7b).

In a multi-story building, it is possible to connect walls of different stories easily, by drilling the floors to allow the vertical loops to pass through them. Drilling is also useful at the building corners (Figure 8a) and wall intersections (Figure 8b), to connect orthogonal walls together.

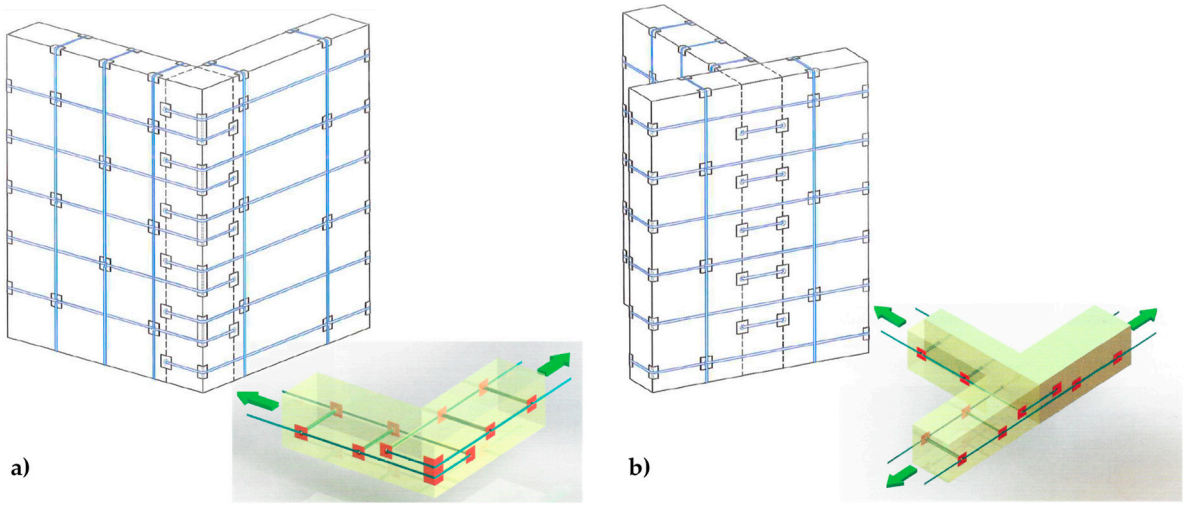

Figure 8. Connections between orthogonal walls, with details of the arrangement of the ribbons in the thickness: a) at a building corner; b) at an intersection between walls.

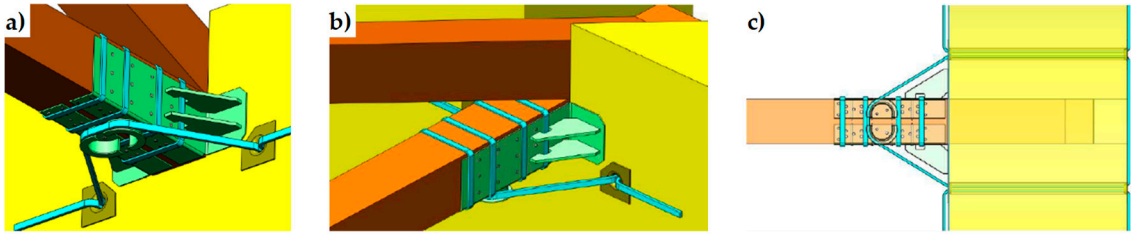

Figure 9. Arrangement of straps to connect perimeter walls to wooden trusses: a) axonometric view from below; b) axonometric view from above; c) plan view.

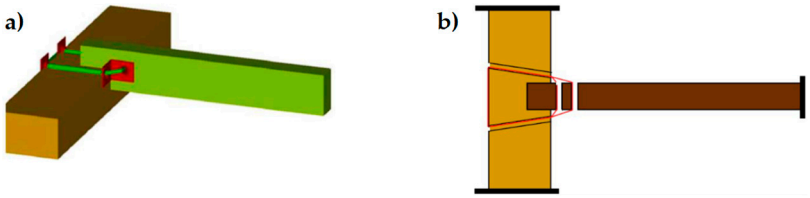

Figure 10. Arrangement of straps to connect perimeter walls to wooden beams: a) axonometric view from above; b) plan view.

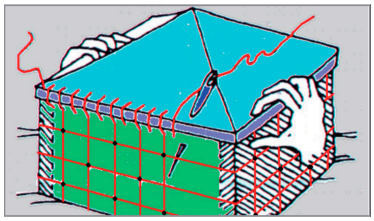

Figure 11. Box-type behavior supplied to the building by the CAM system [10].

Preprints (www.preprints.org) | NOT PEER-REVIEWED | Posted: 20 February 2019 doi:10.20944/preprints201902.0194.v1

Peer-reviewed version available at Materials 2019, 12, 1171; doi:10.3390/ma12071171

Moreover, it is possible to connect the perimeter walls to wooden trusses (Figure 9), wooden beams (Figure 10) and metallic beams (Figure 4a), thus improving the wall to roof and wall to floor connections. Improving the structural connections gives continuity to the retrofitting system, making it possible to connect all the structural elements together. Therefore, the CAM system is able to provide the building with an overall box-type behavior (Figure 11).

The holes drilled in the masonry wall behave as cylindrical hinges (Figure 12a), even when we fill the holes with mortar after retrofitting. This is particularly detrimental to the rectangular arrangement of the CAM system. Actually, the straps form unbraced rectangular frame structures with hinged nodes (Figure 12b), both in the plane of the wall and the thickness of the wall. Since the unbraced rectangular frame structures are not able to withstand lateral forces and sway laterally, the rectangular arrangement of the CAM system is labile along both the in-plane (Figure 13a) and transverse directions of the wall (Figure 13b). In particular, it is not able to counteract the out-of-plane loads, that is, is not suitable for increasing the ultimate load of collapse when the directional properties of the earthquake involve a hammering action of floors on the walls. This is why we need to combine the CAM system with other reinforcement techniques for increasing the wall resistance to hammering actions.

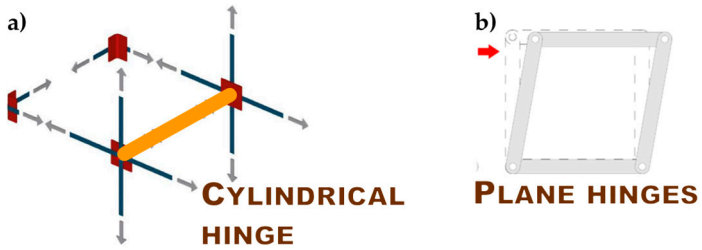

Figure 12. Hinged mechanisms: a) in the wall thickness; b) in the wall plane.

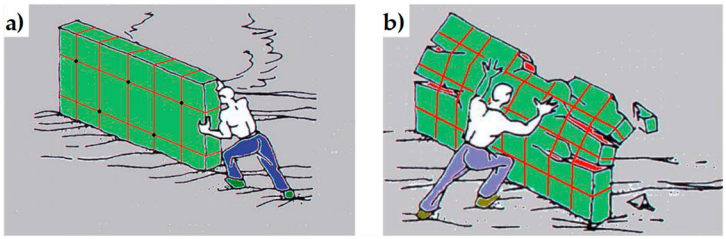

Figure 13. Loading of a wall reinforced with the CAM system: a) shear loading in the midplane [13]; b) out-of-plane loading [13].

3. Techniques of cross bracing in the thickness of the wall

3.1. Re-arrangement of the CAM straps

In [14], we have shown that it is possible to re-arrange the CAM straps to find a statically determined strap configuration for lateral loads, in order to increase the load-bearing capacity for shear loads. In fact, by arranging the straps along the two principal directions of stress for shear stress (forming angles of ±45° with respect to the horizontal direction [15]), we obtain a cross bracing effect in the plane of the wall (Figure 14).

The idea of turning the straps in search of a cross bracing effect suggests us a possible application to counteract out-of-plane displacements: to gain an effect of cross bracing in the thickness, we should drill the wall along directions not orthogonal to the wall, with positive and negative slopes alternately (Figure 15a). Though theoretically possible, this solution is impracticable because too complicated from the technological point of view. Therefore, to increase the load-bearing capacity for out-of-plane loads we must develop some alternative solutions.

Peer-reviewed version available at Materials 2019, 12, 1171; doi:10.3390/ma12071171

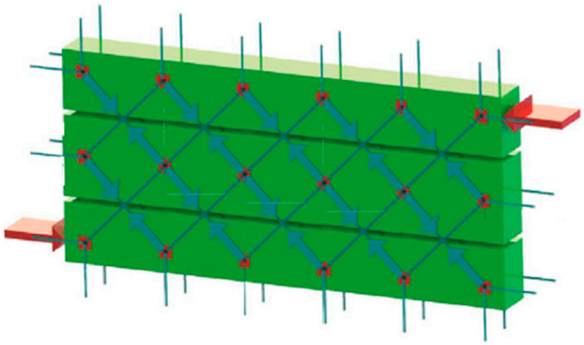

Figure 14. Optimized arrangement of straps for in-plane shear loads.

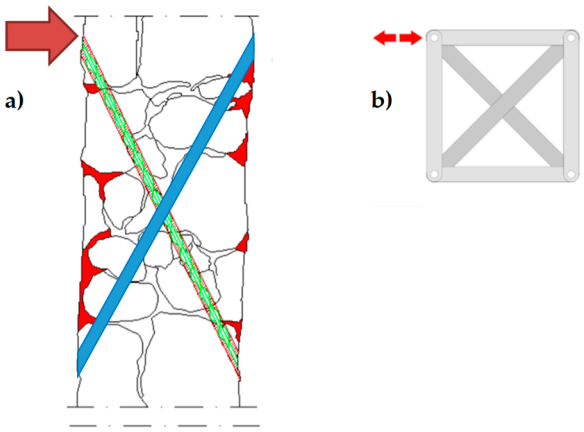

Figure 15. a) Inclined perforations to achieve a cross-bracing effect in the thickness; b) Behavior scheme of a braced rectangular frame structures with hinged nodes.

3.2. *Application of the CAM system together with CFRP strips*

The second technique exploits the capacity of the CAM system of establishing a transversal link with designable stiffness. In fact, once we have chosen the type of stainless steel and the cross-section of the straps, we can increase the stiffness of the transversal link by increasing the number of straps per loop (up to a maximum of 4 straps per loop).

It is precisely the possibility of designing the stiffness of the transversal link that allows us to use the CAM system to build an embedded buttress. If fact, if we wanted to build an embedded buttress with a traditional technique, we would probably incorporate an FRP I-beam in the thickness of the wall, placing the two flanges vertically on the two faces of the wall to maximize the moment of inertia. As well known, the cross-section of a bent I-beam (Figure 16a) behaves as two ideal point-masses, linked by a stiffness constraint (Figure 16b). The idea underlying this paper is that it is possible to reverse the path in Figure 16, moving from two masses, linked by a stiffness constraint, to an (ideal) beam under bending load. In this case, if we were able to establish a stiffness constraint between two masses placed on the two sides of the masonry wall, we could obtain an (ideal) embedded buttress without having to cut the masonry wall to insert a beam.

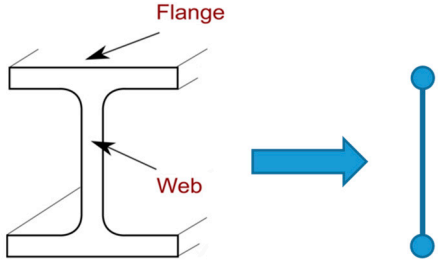

Figure 16. Ideal scheme of behavior of an I-beam: two point masses, linked by a stiffness constraint.

Peer-reviewed version available at Materials 2019, 12, 1171; doi:10.3390/ma12071171

Following this inspiring idea, we decided to exploit the stiffness constraint provided by the CAM straps to link together the CFRP strips bonded on the two opposite sides of a masonry wall, so that the two CFRP strips behave like the two flanges of an ideal CFRP I-beam (Figure 17). To this aim, we used some straps of a continuous CAM net to tie together the CFRP strips bonded on the two opposite sides of the masonry wall, one in front of the other as in Figure 17. Since the CAM net crosses the floors easily, establishing effective wall-to-wall connections (Section 2), the ideal I-beam can extend to the entire height of the building, thus counteracting the hammering actions of the floors.

In the explanatory scheme shown in Figure 17, the masonry wall enclosed between the two CFRP strip acts as a lost formwork, as it serves to define the distance between the two flanges of the ideal I-beam and remains within the construction. The thicker the masonry wall, the higher the web and, consequently, the greater the moment of inertia of the ideal I-beam [16].

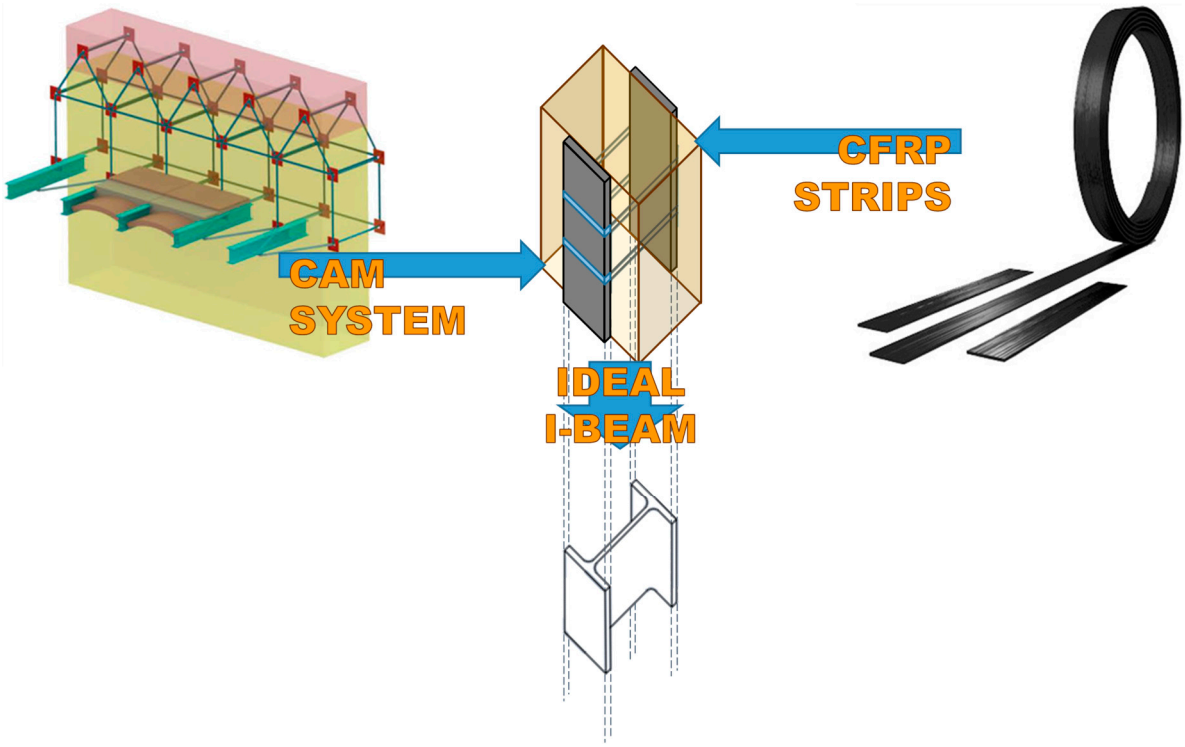

Figure 17. How the ribbons of the CAM system and the CFRP strips work together to provide us with a bracing effect in the thickness, similar to that given by an embedded I-beam acting as a buttress.

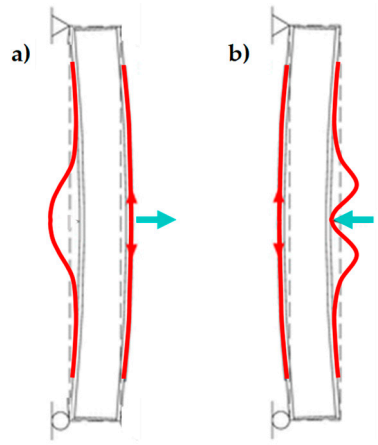

Figure 18. Buckling of the compressed CFRP strip, when: a) the load is on the side opposite to that of buckling; b) the load is on the side of buckling and pushes on the compressed CFRP strip.

Preprints (www.preprints.org) | NOT PEER-REVIEWED | Posted: 20 February 2019 doi:10.20944/preprints201902.0194.v1

Peer-reviewed version available at Materials 2019, 12, 1171; doi:10.3390/ma12071171

Before tying the two strips of CFRP together, the strips work independently, in the sense that there is no bound between them. In particular, the ultimate flexural strength of the masonry wall depends on the strip applied on the stretched side. In fact, due to buckling, the strip on the compressed side of a bent wall undergoes delamination before the stretched strip (Figure 18).

The delamination of the stretched strip occurs when the shear forces at the strip-beam interface exceed a limit value. In absence of straps, as in Figure 18, the limit value depends on the properties of the resin, which establishes a chemical bond between the strip and the beam.

Figure 19 explains the behavior of the other possible type of bond between two bodies, the physical bond, when a normal force presses the two bodies together. In particular, in Figure 19:

- **P** is the weight force, exerted by body 1 on the support plane;
- **N** is the normal reaction force, equal and opposite to **P**, exerted by the support plane on body 1;
- **T** is the shear force, exerted by the hanging body (body 2) on the support plane;
- **A** is the friction force, developed by the support plane as a reaction to **T**: in static conditions, **A** is equal and opposite to **T**;
- **F** is the resultant force acting on the support plane (the components of **F** are **P** and **T**);
- **Φ** is the resultant force acting on body 1 (the components of **Φ** are **N** and **A**);
- $\alpha = \tan^{-1} A/N$ is the angle formed by **Φ** with the direction orthogonal to the support plane;
- ϕ_s is the angle of static friction, that is, the maximum inclination angle of the support plane before which body 1 will begin sliding on it;
- $\tan \phi_s$ is the coefficient of static friction, a dimensionless scalar value that describes the maximum ratio of the force of friction between two bodies at rest relative to each other and the force pressing them together;
- $\tan \phi_d$ is the coefficient of kinetic friction, that is, the ratio of the force of friction between two bodies in relative motion and the force pressing them together.

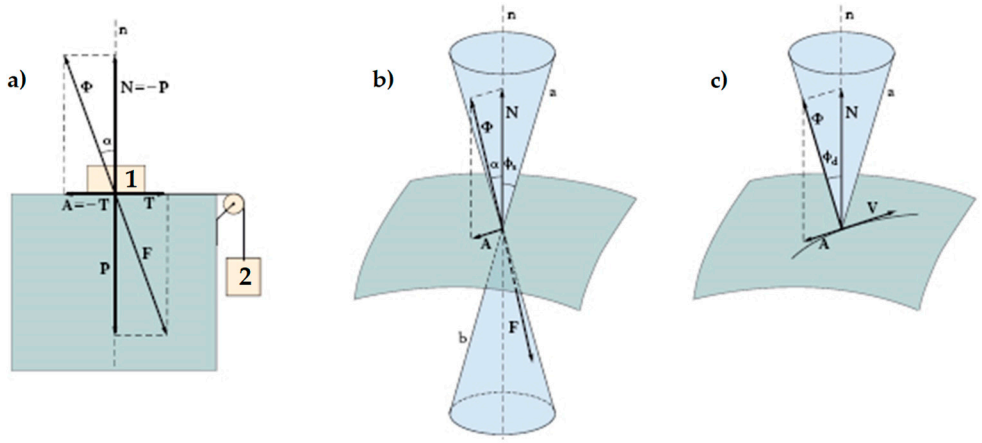

Figure 19. a) Forces at the interface between a body at rest (body 1) and its support plane; b) Cone of static friction; c) Cone of kinetic friction.

Both coefficients of friction depend on the pair of surfaces in contact. For a given pair of surfaces, the coefficient of static friction is usually higher than the coefficient of kinetic friction.

The angle ϕ_s is equal to half the aperture of the static friction cone (the right circular double cone in Figure 19b). For bodies at rest relative to each other, the angle α cannot never exceed ϕ_s.

If Φ falls within the cone of static friction, there is no relative displacement between body 1 and the support plane. When α equals ϕ_s, Φ reaches the lateral surface of the cone of static friction. This limit condition separates the state at rest from the state of motion: as soon as Φ touches the lateral surface, the friction force A decreases so that Φ lies down along a generatrix of the lateral surface of the kinetic friction cone (the right circular cone in Figure 19c). Therefore, **A** and **T** are no longer vectors of equal magnitude and body 1 starts to slide along the direction of **T**.

Peer-reviewed version available at Materials 2019, 12, 1171; doi:10.3390/ma12071171

Well, when the straps tie the CFRP strips together, the straps add a physical bond to the chemical bond provided by the resin, because the pre-tension of the straps presses the CFRP strips against the masonry wall (Figure 20a) in the same way as the compression force of Figure 20b presses body 1 against the support plane.

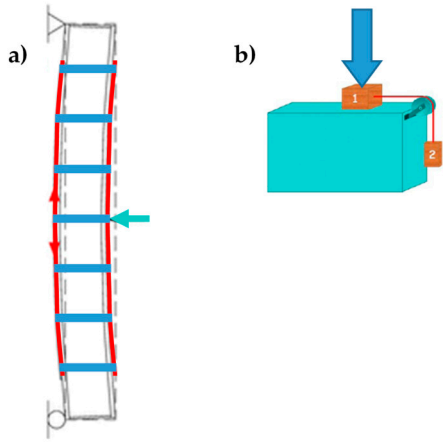

Figure 20. a) The straps delay delamination on both sides of the beam; b) Scheme of the physical bond added by the straps: the compression force represents the action of the straps on the CFRP strips.

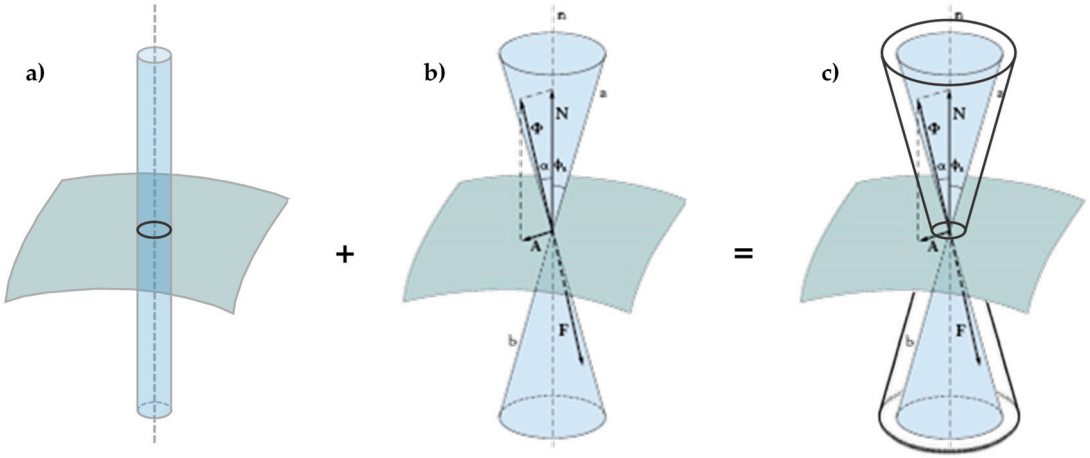

Figure 21. a) Limit surface of the chemical bond: the shear forces determine the limit condition, independently of the compression forces; b) Cone of static friction; c) Cone of cohesive static friction.

As far as the transition from the state at rest to the state of motion is concerned, when we combine the cylinder of Figure 21a, which represents the limit surface of the chemical bond provided by the resin, with the cone of static friction (Figure 21b), we obtain the right circular double truncated cone of Figure 21c. Therefore, Figure 21c represents the limit surface of the cohesive physical bond, provided by the resin and the straps acting simultaneously (cone of cohesive static friction).

Compared to the chemical bond, the advantage of the cohesive physical bond is twofold:

- On the compressed side, the straps prevent the buckling of the CFRP strip, the main cause of delamination on that side.
- On the stretched side, the compression forces exerted by the straps on the CFRP strip modify the shape of the limit surface, from the cylinder of Figure 21a to the double truncated cone of Figure 21c. As a result, the CFRP strip can withstand higher shear forces before the head of **Φ** touches the limit surface. Since the shear forces depend on the bending load linearly, this ultimately means that the stretched CFRP strip will undergo delamination for higher values of the bending load. Therefore, the strapping delays the delamination on the stretched side.

Peer-reviewed version available at *Materials* **2019**, *12*, 1171; doi:10.3390/ma12071171

The masonry wall benefits from the bracing effect provided by the ideal I-beam until the stretched strip undergoes delamination. After that, the actual behavior of the retrofitted system depends on the stiffness of the transversal link provided by the straps (see Section 4.5).

4. Experimental program

4.1. Funnel plates and rounded angles

The experimental program on the effectiveness of the combined technique discussed in Section 3.2 includes the design of new protective elements for the loop corners. The adopted solution, shown in Figure 22, consists of 3D printed elements, made with PLA filament, which substitute the CAM protective elements of Figure 23.

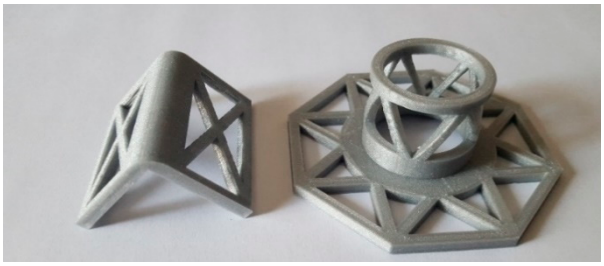

Figure 22. 3D printed funnel plates and rounded angles.

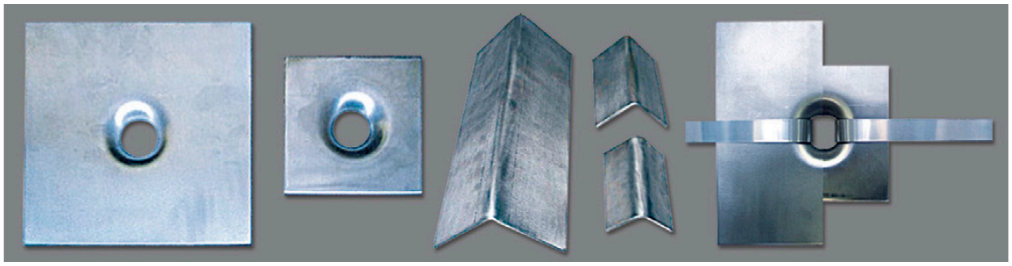

Figure 23. Protective elements of the CAM system [6].

PLA (Polylactic Acid) is one of the two most commonly used filaments in FDM (fused deposition modeling) 3D printing, with the other being ABS filament. Our choice fell on the PLA filament for environmental reasons. In fact, PLA filament is one of the most eco-friendly 3D printer materials available, because the polymerized lactic acid comes from annually renewable resources (cornstarch, tapioca roots, sugarcane or other sugar-containing crops). Furthermore, it requires less energy to process compared to traditional (petroleum-based) plastics.

PLA is a thermoplastic, biodegradable and non-toxic polyester. During printing, the PLA filament emits a pleasant sugary scent and releases only carbon dioxide into the air. Moreover, one can simply discard unwanted PLA printed objects in the soil or aggressive natural environments, where they will naturally decompose. For example, an item made of PLA plastic in the ocean has a degradation time of the order of six months to two years, while conventional plastics take from 500 to 1,000 years to degrade.

It is important to point out that, although PLA will degrade in an exposed natural environment, it is very robust in any normal application or when adequately protected against degradation: its stiffness and hardness make it similar to iron.

Both the 3D printed plates and angles have rounded external corners – where they adhere to the straps – and internal corners at 90°, to improve the coupling with the wall (Figure 22). The rounded external corner prevents the strap from bending too tightly and tearing during pre-tensioning. It is worth noting that only 3D printing can provide us with protective elements with these geometric characteristics, as it is impossible to obtain different shapes for external and internal corners with the traditional hot forming technique used for the CAM elements in Figure 23.

Peer-reviewed version available at Materials 2019, 12, 1171; doi:10.3390/ma12071171

Finally, the flat parts of the 3D printed protective elements have a truss shape. When positioning the protective elements, the mortar fills the truss structure: this improves the adherence between the masonry wall and the protective elements, once the mortar has hardened (Figure 24).

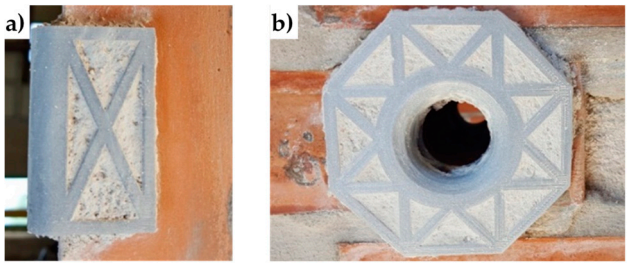

Figure 24. 3D printed elements after placing in place: a) rounded angles; b) funnel plates.

4.2. Straps and seals

Figure 25 shows the stainless steel straps and seals of the CAM system. The comparison between the stress/strain curves of the displacement controlled tensile tests, performed on CAM straps with and without seals (Figure 26), shows that the CAM junction is weaker than the straps. In fact, the seal of the CAM system breaks at a load that is lower than the breaking load of the strap. Consequently, the strength of a strap clamped by the CAM system is lower than the strength of the strap alone.

Figure 26 also shows that the seal modifies the stiffness of the jointed steel ribbons. In fact, the initial slope of the stress/strain curves for the jointed specimens is lower than for the specimens without junctions, which means that applying a seal decreases the stiffness of the tying system.

Finally, the failure mechanism of the jointed specimens of Figure 26 is brittle, as the specimens break shortly after the point of maximum stress. This causes the CAM junctions to break almost suddenly.

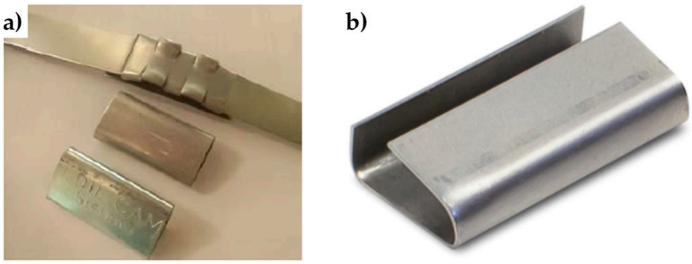

Figure 25. a) Steel ribbons and seals of the patented CAM system [10]; b) A detail of a CAM seal.

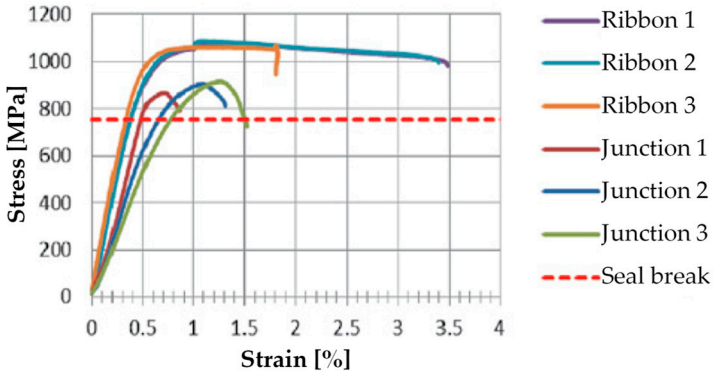

Figure 26. Stress/strain diagrams of the CAM ribbons, with and without seals [6].

Since the brittle junctions do not allow the straps to show signs of warning against the crisis, one of the aims of our experimental program was to equip the tying system with ductile junctions. Figure 27 shows the stainless steel seal of the experimental program, used to clamp 19 mm wide and 1 mm

Peer-reviewed version available at Materials 2019, 12, 1171; doi:10.3390/ma12071171

thick stainless steel straps. Since these straps are not of the type patented with the CAM system, we will call them "the CAM-like straps".

To investigate the behavior of the new junction, we performed tensile tests under displacement control on the following 4 specimens (Figure 28), where the steel ribbons were cut by the stainless steel straps of the experimental program:

- Specimen L2, consisting of a steel ribbon without junction;
- Specimen L3, consisting of a steel ribbon without junction;
- Specimen S2, consisting of 2 pieces of steel ribbon, fastened together by 1 seal;
- Specimen S3, consisting of 2 pieces of steel ribbon, fastened together by 2 seals;

Figure 27. The seal used in the experimental program.

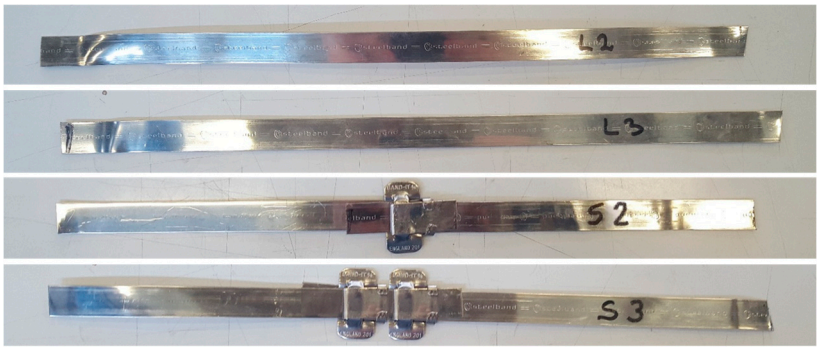

Figure 28. The four specimen for the characterization of the CAM-like ribbons and new junctions.

The stress/strain diagrams in Figure 29 clearly show that the strength of the CAM-like straps is much lower than the strength of the straps used with the patented CAM system (Figure 26).

As far as the initial stiffness is concerned, the application of the seal decreases the stiffness of the tying system even for the new junction. In fact, in Figure 29 the initial slope of the stress/strain diagrams of Specimens S2 and S3 is lower than the initial slope of the stress/strain diagrams of Specimens L2 and L3.

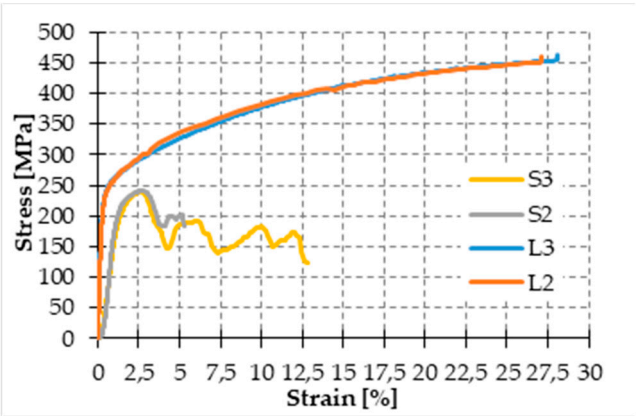

Figure 29. Stress/strain diagrams of the CAM-like ribbons, with and without seals.

Peer-reviewed version available at Materials 2019, 12, 1171; doi:10.3390/ma12071171

Moreover, the yield strength of Specimens S2 and S3 is almost the same as the yield strength of Specimens L2 and L3. The maximum stress of Specimens S2 and S3, on the contrary, is lower than the maximum stress of Specimens L2 and L3. Thus, also clamping by means of the seal in Figure 27 decreases the strength of the straps. Nevertheless, now the behavior of the junction is ductile, as a stage of oscillatory stress separates the maximum stress from the ultimate stress (Figure 29). Therefore, the junction no longer breaks fragilely.

The ductile behavior of the jointed steel ribbons is a consequence of the sliding that takes place – into the seal – between the ends of the straps. The sliding into the seal is also the main cause of the crisis: while in the CAM system the junction fails due to the breaking of the seal, this second time the junction fails when one of the two ends slips off from the seal (Figure 30). This failure mechanism also explains why the oscillatory stage of Specimen S3 (with 2 seals) is longer than the oscillatory stage of Specimen S2 (with just 1 seal): since 2 seals are more effective than just 1 seal in counteracting the sliding, unfastening the junction of the specimen with 2 seals needs more time. In other words, the junction of Specimen S3 withstands a higher relative displacement than Specimen S2.

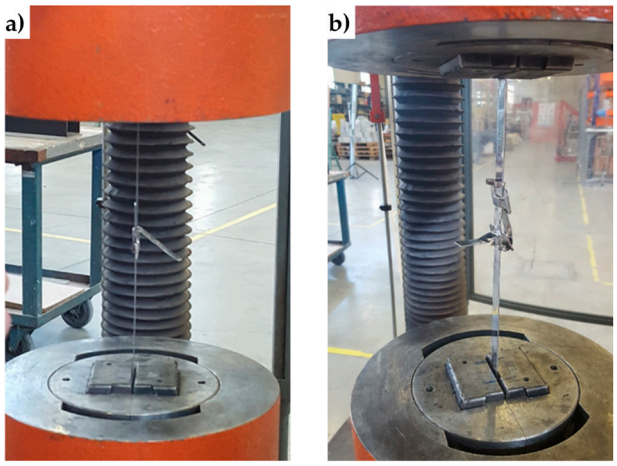

Figure 30. How the new junction unfastens, with: a) 1 seal; b) 2 seals.

It is worth noting that even leaving longer ends when cutting the straps allows us to delay unfastening, as happens when using two seals. In the specific case of our experimental program, however, we decided not to use either longer ends or two seals, because an ultimate strain of more than 5% (achieved with Specimen S2) is already satisfactory for our purposes.

4.3. Mechanical characterization of bricks and mortar

The mechanical characterization of bricks took place by performing uniaxial compression tests on 6 brick specimens (Figure 31a), cut from 3 different bricks of the experimental program. The methods used to cut and dry the specimens and carry out the uniaxial compression tests comply with UNI EN 772-1. Table 1 collects the results of the compression tests.

The mortar of the experimental program is a single-component, fiber-reinforced, sulfate-resistant, shrinkage controlled mortar, useful for repairing and reinforcing concrete structures, mixed masonry, historic walls and curtain walls.

The mechanical characterization of the mortar complied the specifications provided by UNI EN 1015-11/2007, which establishes to perform both three-point bending flexural tests on prismatic specimens and uniaxial compression tests on cubic specimens. Figure 32 shows the 6 prismatic specimens of the experimental program. After the flexural tests, each prismatic specimen provided us with two cubes for the uniaxial compression test.

Table 2 shows the results of the three-point bending flexural tests on the 6 prismatic specimens and the uniaxial compression tests on the 12 cubic specimens (EN 196-1:2016). Since the average compressive strength is equal to 19.66 N/mm^2, the mortar is of the M20 type.

Peer-reviewed version available at Materials 2019, 12, 1171; doi:10.3390/ma12071171

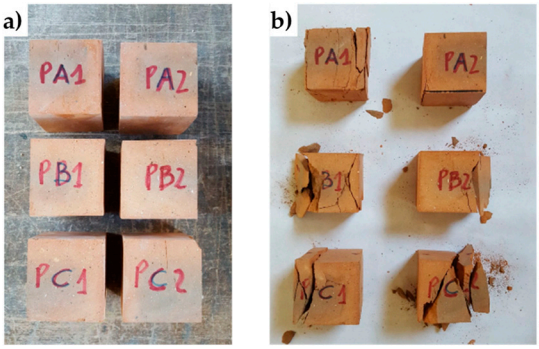

Figure 31. The 6 specimens tested for brick characterization: a) before the test; b) after the test.

Table 1. Geometric and mechanical characteristics of the 6 brick specimens.

Specimen	Dimensions [mm]	Weight [g]	Breaking load [N]	Compressive strength [N/mm²]	Normalized compressive strength [N/mm²]
PA1	55×54×55	296.1	116436	39.63165	34.47953
PA2	57×57×55	317.8	165730	50.91128	44.29281
PB1	55×53×55	297.5	146733	49.62439	43.17322
PB2	56×55×57	319.2	142681	46.09916	40.10627
PC1	56×53×56	310.5	144933	47.77687	41.56587
PC2	56×55×56	317.1	149422	48.14767	41.88848

Figure 32. The 6 specimens for three-point bending flexural tests on mortar.

Table 2. Geometric and mechanical characteristics of the mortar specimens.

Specimens of the flexural tests	Dimensions [mm]	Weight [g]	Breaking load in bending [N]	Flexural Strength [N/mm²]	Specimens of the compression tests	Breaking load in compression [N]	Compressive Strength [N/mm²]
P1	40×40×160	466.42	1758	4.12	P1A	30530	19.08
					P1B	36730	22.96
P2	40×40×160	469.81	1838	4.31	P2A	30980	19.36
					P2B	30930	19.33
P3	40×40×160	470.42	1443	3.38	P3A	27500	17.19
					P3B	28530	17.83
P4	40×40×160	459.63	1885	4.42	P4A	34544	21.59
					P4B	27730	17.33
P5	40×40×160	463.81	1990	4.66	P5A	33880	21.18
					P5B	35200	22.00
P6	40×40×160	462.01	1598	3.75	P6A	30400	19.00
					P6B	30450	19.03

Peer-reviewed version available at Materials 2019, 12, 1171; doi:10.3390/ma12071171

4.4. Specimens W1, W2 and W3

Figure 33 shows the first set of 3 specimens of the experimental program, where:

- The three brick walls are of identical dimensions (50 × 146 × 23 cm).
- The bricks are of the Bolognese type: they measure 24.5 cm in length, 5.5 cm in height and 11 cm in depth. Figure 34 shows how we arranged the bricks in the odd and even rows. In particular, in the odd rows we adjusted the length of the end bricks to fit the thickness of the wall. For the mechanical characteristics of the bricks, see Section 4.3.
- Specimen W1 is a drilled masonry wall, with the holes arranged in quincunxes. This choice minimizes the number of holes and gives rise to two three-dimensional nets of straps, staggered along the horizontal and vertical directions.
- Specimen W2 is an undrilled wall, where we applied some CFRP strips along the two vertical centerlines of the main faces, specifically, two strips side by side for each centerline. The CFRP strips are 25 mm wide and 1.2 mm thick.
- Specimen W3 is a drilled wall, with the holes arranged in quincunxes, where we applied both the staggered nets of straps and the side-by-side CFRP strips along the vertical centerlines. In particular, we used some straps of both three-dimensional nets to tie the strips together.

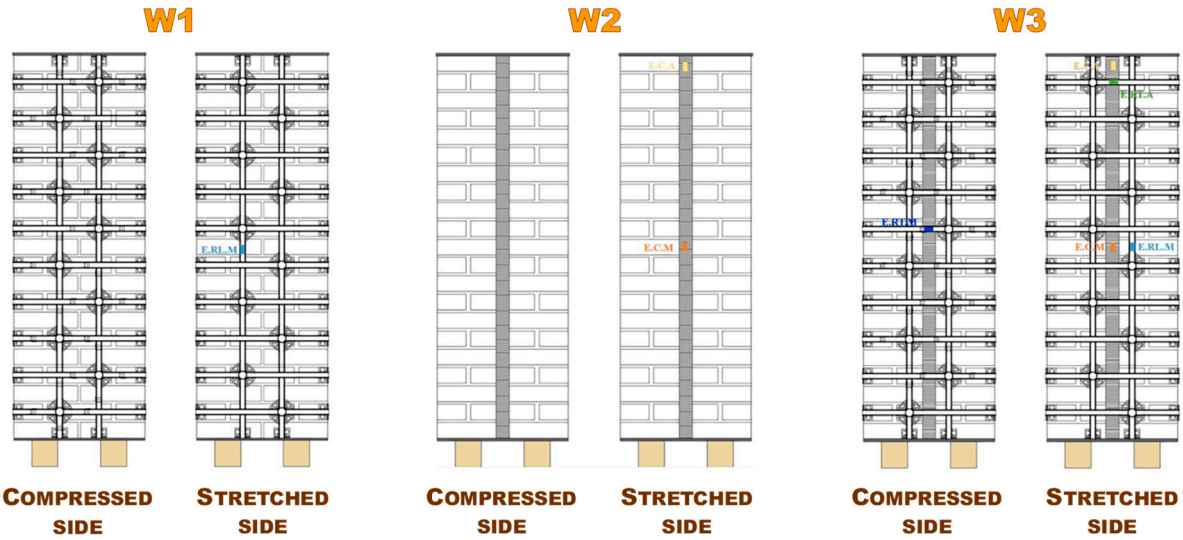

Figure 33. Strengthening schemes of Specimens W1, W2 and W3.

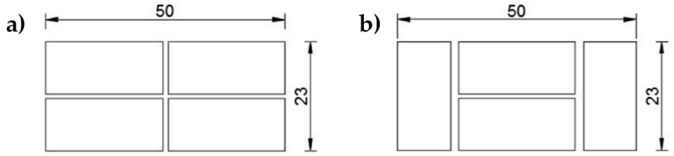

Figure 34. Arrangement of the bricks in the rows (all measures in *cm*): a) odd rows; b) even rows.

Figure 35. a) Preparation of the bricks to be drilled; b) Detail of a brick after drilling.

Peer-reviewed version available at Materials 2019, 12, 1171; doi:10.3390/ma12071171

- Drilling of the bricks for Specimens W1 and W3 took place on the individual bricks (Figure 35a), before starting to build the walls. This allowed us not to face damages or stability problems of the walls during drilling. The core drill used to remove the brick cores has a diameter of 4 cm (Figure 35b).
- The protective elements at the loop corners of Specimens W1 and W3 are those of the research activity discussed in Section 4.1.
- The straps used for the active confinement of Specimens W1 and W3 are the CAM-like straps described in Section 4.2.
- The stainless steel seals used for Specimens W1 and W3 are those described in Section 4.2.
- For both Specimens W1 and W3, we used just one strap per loop.
- The strapping of Specimens W1 and W3 took place in two steps, first arranging all the straps spanning along the short direction (transverse straps) and, secondly, completing the strapping with the straps spanning along the long direction (longitudinal straps). This allows the longitudinal straps to pass over the transverse straps at the intersections between the straps (Figure 36c). As a result, the pre-tension of the longitudinal straps pushes the transverse straps against the wall, allowing the transverse straps to block the CFRP strips more firmly. Therefore, the transverse straps load the CFPR strips symmetrically, according to schemes a) and b) of Figure 36, alternatively.
- The tool used to pre-tension the straps of Specimens W1 and W3 is the manual strapping tool for steel shown in Figure 37.
- We instrumented the three specimens with strain gauges on both sides (Figure 33).
- After curing and instrumentation, we overturned the 3 specimens in horizontal configuration (Figure 38b).
- We placed some flat steel bars on the central cross-sections of the three specimens, in order to distribute the load given by the testing machine. The arrangement of the flat steel bars allowed the load not to compress the straps and, in Specimens W2 and W3, the upper CFRP strips (Figure 39).
- We performed three-point bending flexural tests under in displacement control on the three specimens, by using some Linear Variable Differential Transformers (LVDTs) to acquire the displacements at the ends and the middle point on the lower faces.

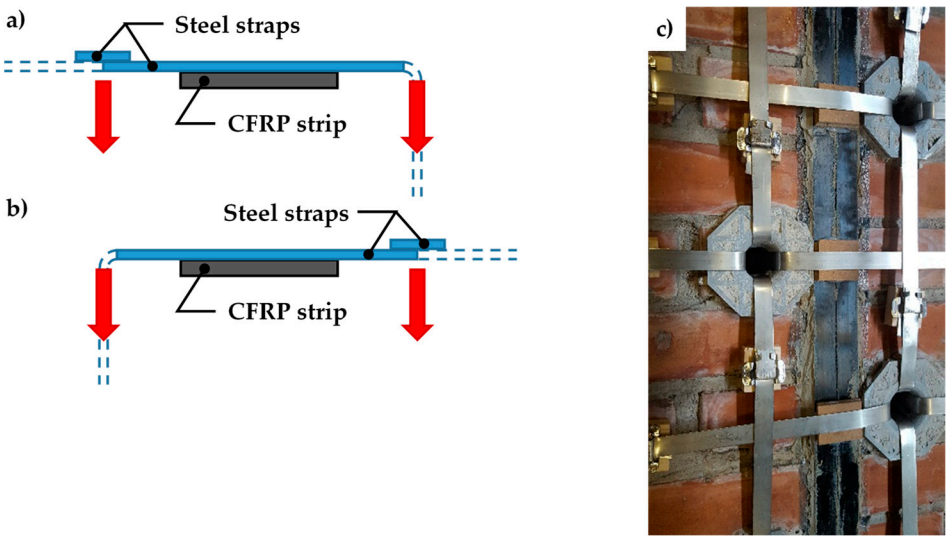

Figure 36. a) Cross-section view: the longitudinal strap pushes down on the transverse strap to the left of the CFRP strip (not to scale); b) Cross-section view: the longitudinal strap pushes down on the transverse strap to the right of the CFRP strip (not to scale); c) Detail of the intersections between the straps: the arrangement of the transverse straps follows the scheme sequence a, b, a.

Peer-reviewed version available at Materials 2019, 12, 1171; doi:10.3390/ma12071171

Figure 37. Manual strapping tool for steel.

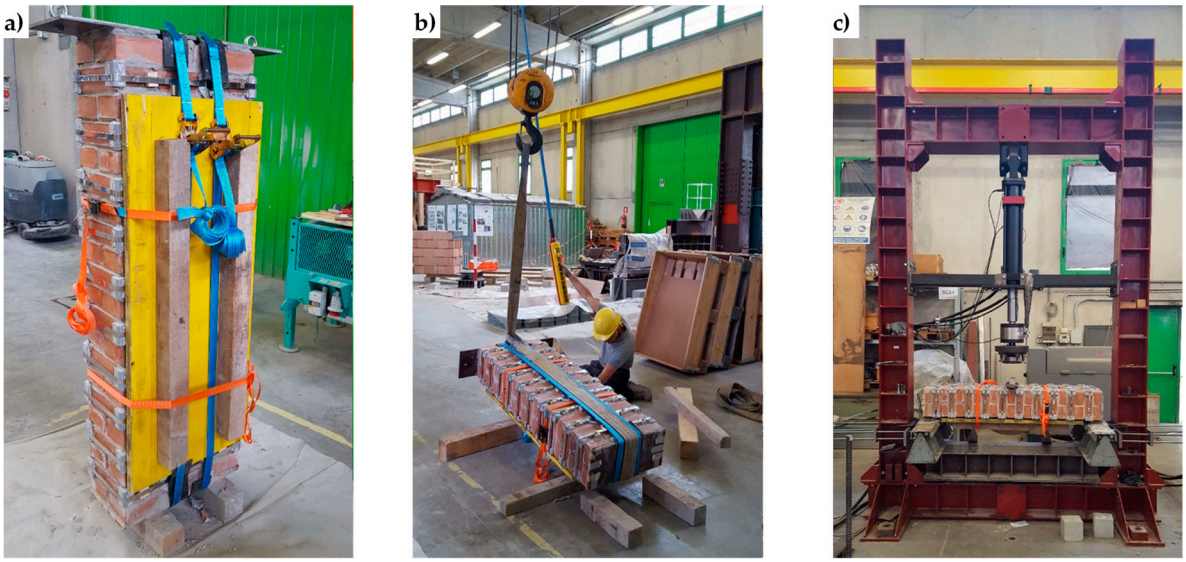

Figure 38. Specimen handling: a) harness; b) overturning; c) positioning on the testing machine.

Figure 39. Arrangement of the flat steel bars on the central cross-section.

In [16], we have already provided some early results on the effectiveness of the combined technique discussed in Section 3.2. Here, we will focus on the post-delamination behavior of a masonry wall after retrofitting by the combined technique. In particular, we will show further experimental results on the strapped masonry walls, to answer the question on whether the stiffness of the transversal link modifies the post-delamination behavior or not.

The increase in ductility is the most important result with regard to the out-of-plane behavior of strapped masonry walls. Actually, since the strength of the steel ribbons is much greater than the masonry strength, the straps continue to wrap masonry even after masonry crushing. This is of fundamental importance in real buildings, as people do not risk that some part of the structure will hit them, due to the building collapse. Therefore, the strapping acts as a reinforcement system before the structural damage occurs and a protection device after the structural damage had occurred.

Peer-reviewed version available at *Materials* **2019**, *12*, 1171; doi:10.3390/ma12071171

The mechanism of safeguarding life allowed by strapping is particularly evident in Figure 40, which is a snapshot of Specimen W1, taken at the end of the test: although the internal hinge of Figure 2 has formed and provided a large relative rotation, the longitudinal straps still keep the beam in equilibrium. Actually, Specimen W1 never collapsed during the flexural test: to avoid instrumentation damages, the operator had to stop the test for a vertical displacement of the loading piston of 12.124 cm (Figure 41), while the specimen would have withstood further increases in vertical displacement. When the operator stopped the flexural test, the specimen was still resisting a load of 5 kN, which is about 65% of the hinge formation load (7.7 kN), and the load was still increasing.

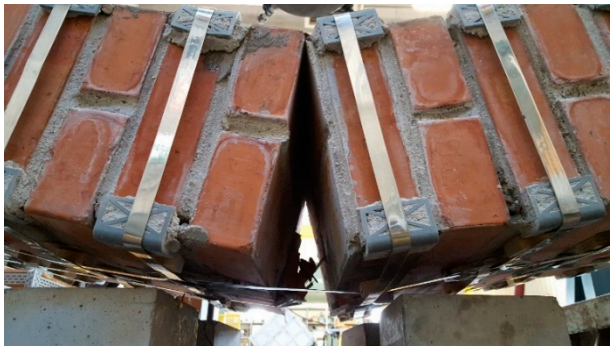

Figure 40. The internal hinge of Specimen W1, which has formed close to the loading piston.

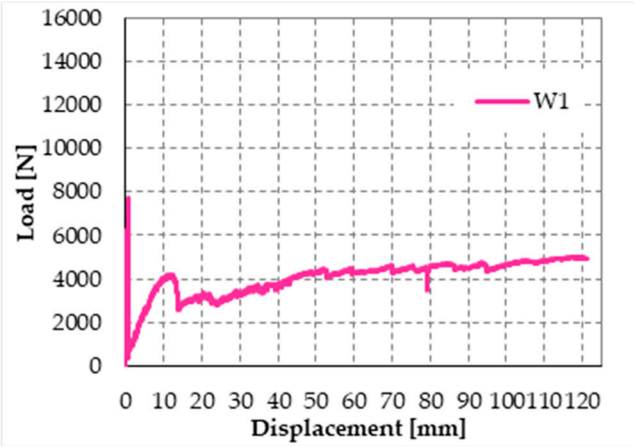

Figure 41. Load/displacement diagram of Specimen W1.

Due to the low pre-tension stress supplied to the straps, the load of hinge formation is the same for the strapped and non-strapped masonry walls. Therefore, the first-peak load of 7.7 kN is the failure load for plain specimens.

Furthermore, the final vertical displacement is about 189% of the vertical displacement at the first peak (0.064 cm), that is, the vertical displacement at failure for plain specimens. This makes the opening of the internal hinge ductile. Finally, the vertical displacement immediately after the first peak in Figure 41 is almost the same as the vertical displacement at the first peak. In other words, the rotation around the internal hinge at the formation of the hinge itself was almost nil. After that, the crack under the internal hinge opened very slowly (Mode I: opening mode), in a controlled manner. It is worth noting that no straps broke during crack opening. Therefore, the tying system is fully adequate to safeguard life even if the strength of the CAM-like straps is much lower than the strength of the patented CAM ribbons (see Figure 26 and Figure 29).

Figure 42 shows the load/displacement diagram for Specimen W2, with a maximum load that is twice the maximum load of Specimen W1. When compared with the load/displacement diagram in Figure 41, Figure 42 shows that the CFRP reinforcement makes the masonry wall stronger, but also much more brittle than the steel straps.

Peer-reviewed version available at Materials 2019, 12, 1171; doi:10.3390/ma12071171

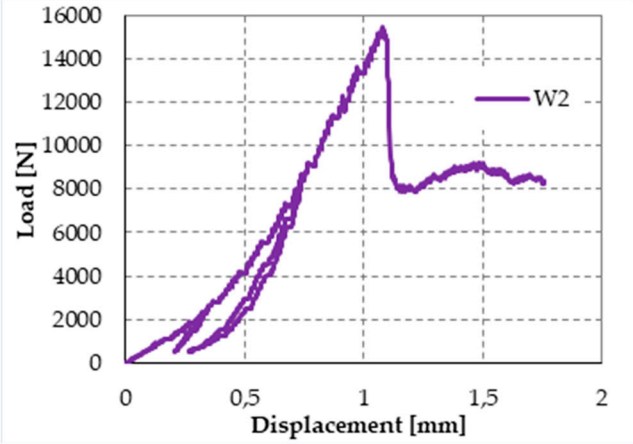

Figure 42. Load/displacement diagram of Specimen W2.

Figure 43. a) Length of the crack for a load of 15 kN (delamination load of the compressed CFRP strip); b) Detail of the delamination on the compressed side, just above the crack.

Figure 44. a) Opening of the crack (Mode I), at the delamination load of the stretched CFRP strip; b) Delamination on the stretched side.

The peak in Figure 42 corresponds to the delamination of the compressed strip, which detached itself starting from the localization cross-section of the internal hinge. Figure 43 is a snapshot of the cross-section where the internal hinge localized, taken at the maximum load (peak load of Figure 42). In particular, the mark in Figure 43a shows the crack length for a load of 15 kN, while Figure 43b is a detail of the CFRP strip delamination, initiated on the compressed side, just above the crack of Figure 43a. As shown by the mark in Figure 43a, initially the crack involved only half the thickness of the specimen. Then, the cross-section underwent a short phase of localized deformations, leading to the increase in vertical displacement – at almost constant load – which characterizes the diagram after the peak of Figure 42: this is the phase in which the cross-section behaved as a plastic hinge. The plastic phase ended with the delamination of the lower CFRP strip, which detached itself starting from the end that was farthest away from the internal hinge (Figure 44b).

Peer-reviewed version available at Materials 2019, 12, 1171; doi:10.3390/ma12071171

The effect provided by the two reinforcement systems that act simultaneously on the masonry wall is twofold, as the combined technique increases both the strength and the ductility. In fact, the maximum load in Figure 45 is comparable to that given by the CFRP strips alone (about twice the failure load of the masonry wall) and the post-peak behavior is as ductile as that offered by the steel straps alone.

It is worth noting that, while the increased ductility of the masonry wall leads to high displacements, it does not involve a high displacement rate, which could be dangerous for people standing in a real building. In fact, at the maximum load of Specimen W3 the load decreases abruptly while the vertical displacement is almost constant (Figure 45). This means that, though the internal hinge forms at the peak, the relative rotation between the two hinged cross-sections is negligible at the peak. Moreover, after the peak the relative rotation increased in a controlled manner, as the steel straps provide the hinge with a plastic behavior. Therefore, the straps allow the internal hinge to achieve high relative rotations without ever losing equilibrium. In other words, Specimen W3 moved along a path of stable equilibrium throughout the duration of the flexural test.

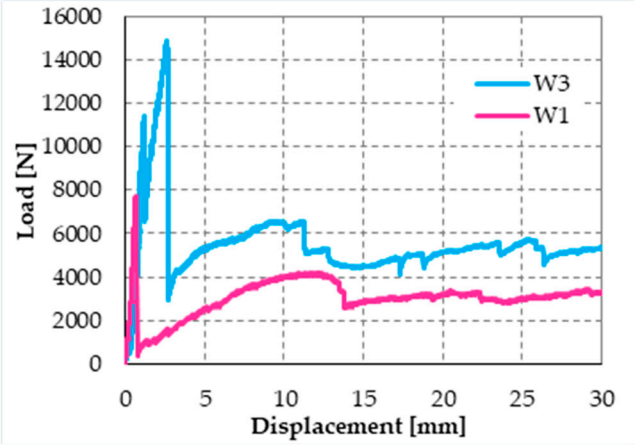

Figure 45. Load/displacement diagrams of Specimens W1 and W3: displacement field truncated at the value of 30 mm.

The post-delamination behavior of Specimen W3 (diagram in Figure 45 after the maximum load) shows that the steel straps retain the delaminated strip, allowing the wall to withstand loads higher than the post-peak loads of Specimen W1 (retrofitted only with steel straps). This means that the wall can benefit of the strengthening effects of both CFRP strips even after the delamination of the stretched strip, although only in part. In other words, the I-beam behavior of the combined technique does not end with the strip delamination: it survives the delamination with a decreased stiffness, which depends on the stiffness of the transversal link. Therefore, increasing the number of straps per loop should increase the load-bearing capacity after delamination, as it increases the stiffness of the transversal link.

To verify this latest statement, we restored Specimen W3 (after testing) and increased the number of straps per loop. We then tested the restored specimen by performing a further three-point bending flexural test in displacement control. This also allowed us to evaluate the effectiveness of the combined technique to restore a damaged structural element.

The new label of Specimen W3 after restoration and strapping is “Specimen W4”.

4.5. Specimen W4

The preparation of Specimen W4 took place as follows:

- Removal of all damaged straps of Specimen W3;
- Cleaning of the specimen surface, in correspondence of the delaminated CFRP strips;
- Removal of the mortar on the cross-section where Specimen W3 opened into two parts;

Peer-reviewed version available at *Materials* **2019**, *12*, 1171; doi:10.3390/ma12071171

- Restoration of the specimen integrity, by walling together the two parts of Specimen W3;
- Curing of the mortar on the restored cross-section;
- Bonding of new CFRP strips on both sides of the specimen;
- Strapping of the specimen according to the scheme of Figure 46, by positioning the vertical straps over the horizontal straps (as for Specimens W1 and W3).

After restoration and strapping, we inverted Specimen W4 to load the face that was on the stretched side of Specimen W3.

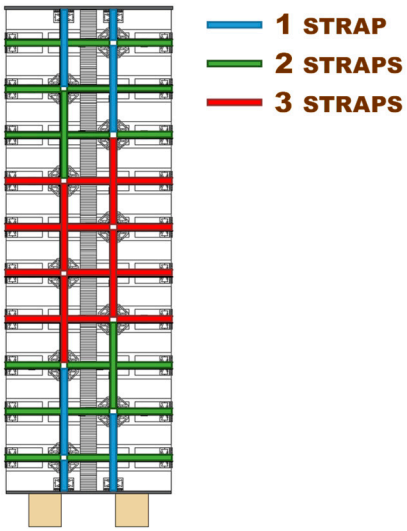

Figure 46. Scheme of strapping for Specimen W4.

Figure 47. a) Specimen W3 at the end of the flexural test; b) Detail of the failure cross-section, where the crack propagation occurred in both Mode I (opening mode) and Mode II (sliding mode).

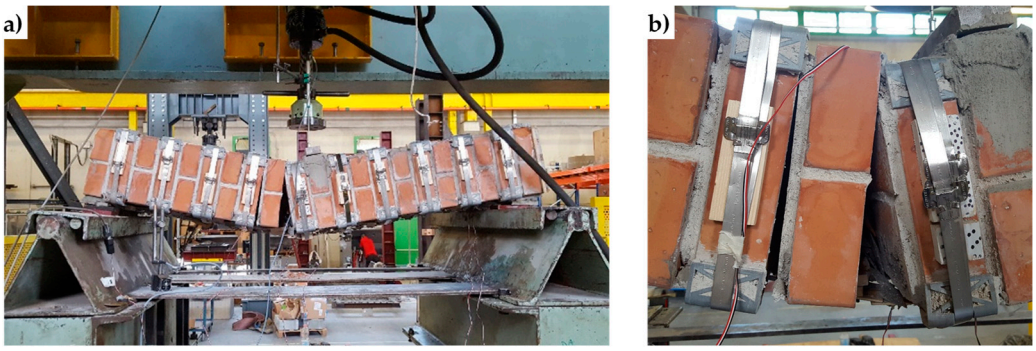

Figure 48. a) Specimen W4 at the end of the flexural test; b) Detail of the 2 failure cross-sections: on the left cross-section the crack propagation occurred in Mode I, while on the right cross-section the crack propagation occurred in both Mode I and Mode II.

Peer-reviewed version available at Materials 2019, 12, 1171; doi:10.3390/ma12071171

Figure 47 and Figure 48 allow us to compare the failure cross-sections of Specimen W3 and Specimen W4: the internal hinge of Specimen W4 localized on the same cross-section as the internal hinge on Specimen W3 (9th mortar bed joint from the left). In addition to this, a second internal hinge has formed for Specimen W4, on the 8th mortar bed joint from the left (Figure 48b). This happened because the strapping provides an infinite degree of internal hyperstaticity to the isostatic static-scheme of the hinged supported I-beam, allowing the formation of multiple plastic hinges on the cross-sections, without ever reaching a labile configuration (until the straps are broken).

The load/displacement diagram of Specimen W4 confirmed the general features of Specimen W1 and Specimen W3: the use of the steel straps made the retrofitted system extremely ductile, to such an extent that the specimen did not experienced collapse up to vertical displacements of the order of 10 cm (Figure 49). Even in the latter case, indeed, the operator had to stop the flexural tests to avoid instrumentation damages, while the specimen would have withstood further increases in displacement. Note that the load/displacement diagram of Specimen W3 in Figure 49 is much shorter than the diagrams of both Specimen W1 and Specimen W4 only because the instrumentation setup prompted the operator to interrupt the flexural test well in advance.

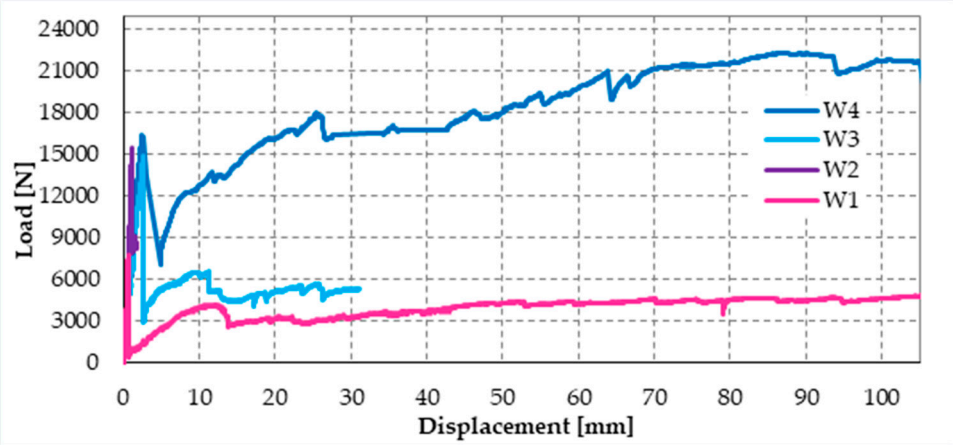

Figure 49. Comparison between the load/displacements diagrams of the 4 specimens.

Figure 49 suggests us some further considerations:

- The restoration was successful, as the delamination load of Specimen W4 is comparable to the delamination load of Specimen W2 (retrofitted only with CFRP strips).
- Specimen W4 underwent delamination at 16.387 kN, while Specimen W3 underwent delamination at 14.904 kN. Therefore, the delamination load after restoration (Specimen W4) is 10% higher than the delamination load before restoration (Specimen W3). As the number of steel straps of Specimen W4 is higher than the number of steel straps of Specimen W3, this confirms that a higher compression load on the CFRP strips delays delamination and increases the delamination load, as discussed in Section 3.2. In fact, a higher compression load increases the magnitude of the normal reaction force, **N**, in Figure 21c, thus increasing the distance between the resultant force acting on a CFRP strip, **Φ**, and the lateral surface of the cone of cohesive static friction.
- Upon delamination of the stretched CFRP strip, the load withstood by Specimen W4 decreased abruptly, but to a lesser extent than for Specimen W3. In fact, the residual load withstood by Specimen W4 after delamination (7.083 kN) is about 236% of the residual load withstood by Specimen W3 (3.004 kN). Once again, the observed behavior depends on having increased the number of steel straps: the friction forces at the interface between CFRP strips and masonry wall – activated by the compression loads provided by the steel straps – counteract the sliding of the delaminated strip. Consequently, the straps continue to tie the two flanges of the ideal I-beam together even after delamination. Moreover, the stiffness of the constraint established between the two flanges depends on the friction forces. Therefore, the greater the number of steel straps,

Peer-reviewed version available at Materials 2019, 12, 1171; doi:10.3390/ma12071171

the greater the friction forces and, consequently, the constraint stiffness. In conclusion, the greater the number of steel straps, the greater the residual load after delamination.

- The positive contribution of increasing the number of steel straps becomes even more evident in the post-delamination stage: after the initial decrease, the post-delamination load of Specimen W4 increases and maintains values that are much higher than those of Specimen W3. Even in the latter case, the increase in load depends on the I-beam behavior of the two CFRP strips, allowed after delamination by the friction forces developed at the interface with the masonry wall.
- In Specimen W4, the post-delamination load increased up to exceed the delamination load, determined for the most part by the stiffness of the CFRP strips. At the displacement value for which the operator stopped the flexural test (22.299 kN), the post-delamination load exceeded the delamination load by more than 36%.

It is worth noting that the longitudinal and transverse straps act on the load/displacement diagram in different ways. In fact, the transverse straps are mainly responsible for the delamination load, while the longitudinal straps are mainly responsible for the post-delamination behavior.

More precisely:

- The pre-tension of the transverse straps delays the delamination of the CFRP strips, by pushing the straps against the wall as shown in Figure 36a and Figure 36b, thus blocking the CFRP strips. Since the (low) pre-tension is provided by imposing a relative displacement between the free ends of the straps, with the relative displacement set by the strapping tool, the pre-tension value and the consequent action on the CFRP strips depend on the stiffness of the straps (the greater the stiffness, the greater the pre-tension).
- The ductility of the longitudinal straps delays the failure of the retrofitted masonry wall, allowing the formation of multiple plastic hinges without ever reaching a labile configuration.

Therefore, having a high ductility is advantageous for the longitudinal straps, while it is disadvantageous for the transverse straps, at least as long as we use a strapping tool in displacement control. Thus, it may be appropriate to use steel with different mechanical properties for the transverse and longitudinal straps.

Finally, using more than one strap in the transverse direction is not as useful as in the longitudinal direction. Actually, strapping a steel ribbon on another strap reduces the pre-tension of the underlying strap. This is not very important for the longitudinal straps, but is detrimental for the transverse straps. In fact, the advantage of using more than one longitudinal strap lies in the cross-sectional increase, which allows the specimen to withstand higher post-delamination loads, regardless of the pre-tension of straps. On the contrary, the transverse straps are all the more effective in pushing the CFRP straps against the wall the greater the average pre-tension of the straps. With reference to Figure 49, this explains why the greater number of transverse straps of Specimen W4 increases the delamination load by only 10% compared to Specimen W3, while the increase in the number of longitudinal straps is much more effective in modifying the post-delamination load.

5. A further combined technique

The second combined technique we propose here is an improvement of the technique discussed in Section 3.2. In fact, the second combined technique arises from the same ideal I-beam scheme that is at the base of the first combined technique, but differs from the latter for the materials used.

The reason that led us to change the materials of the tying system lies in the analysis of the results of Section 4. In particular, on the one hand, our first results showed that the CAM-like straps are actually able to provide an I-beam behavior that is particularly noticeable after delamination but, on the other hand, the delamination load does not increase in a sensitive way. Since we have assumed that the normal stresses at the interface between strips and straps increase the delamination load, due to the friction forces (Figure 20b), we can therefore conclude that stiffer strips would increase the delamination load. This suggested us to replace the steel ribbons with steel wire ropes.

Peer-reviewed version available at *Materials* **2019**, *12*, 1171; doi:10.3390/ma12071171

The use of steel wire ropes instead of steel ribbons leads us to face new problems to fasten the loose ends. The first problem concerns fraying, as the end of a wire rope tends to fray readily, not allowing easy connections. There are different ways of securing the ends of wire ropes to prevent fraying. The most common and useful type of end fitting for a wire rope is the Flemish eye, which consists in turning the end back to form a loop and fixing the loose end back on the wire rope (Figure 50).

Figure 50. A wire rope terminated in a loop (Flemish eye) with a thimble and ferrule.

If the wire rope terminates with a loop, there is a risk that it will bend too tightly when the loop is connected to a device that concentrates the load on a relatively small area. In these cases, a thimble installed inside the loop (Figure 50) is useful to preserve the natural shape of the loop and protect the cable from pinching and abrading on the inside of the loop. The thimble prevents the load from coming into direct contact with the wires.

In Figure 50, a ferrule fixes the loose end of the loop back to the wire rope. Another device for fixing the loose end of the Flemish eye is the wire rope clamp, also called a clip, which consists of a U-shaped bolt, a forged saddle and two nuts (Figure 51). The two layers of wire rope lie in the U-bolt. Then, the saddle fits above the ropes to the bolt (the saddle includes two holes to fit to the U-bolt) and the nuts secure the arrangement in place.

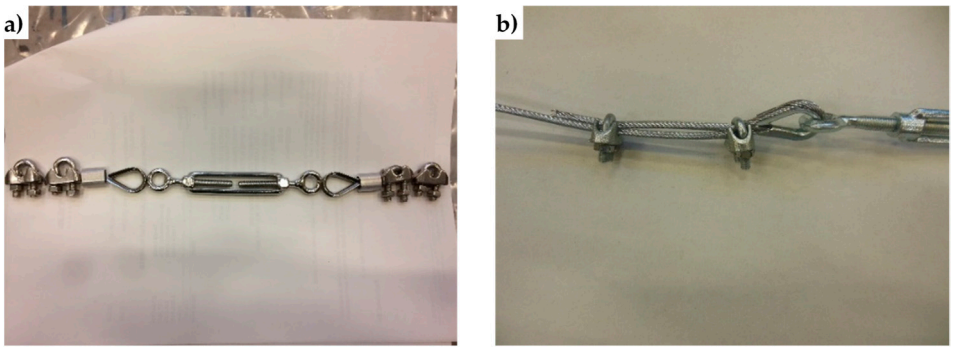

Figure 51. a) The sequence of devices used to fasten the loose ends of the steel wire ropes together, in the second combined technique: an eye-eye turnbuckle in the middle and a series of 2 clips, 1 ferrule and 1 thimble on both sides; b) How to install the clips, with the saddle portion of the clamp assembly placed against the "live" end.

The function of the flat bearing seat and extended prongs of a clip (saddle) is to protect the live or stress-bearing end of the rope against crushing and abuse. Therefore, when installing clips, the saddle portion of the clamp assembly is placed against the load bearing or "live" end (Figure 51b), not against the non-load-bearing or "dead" side of the cable.

The number of clamps needed to terminate a wire rope, usually three or more, depends on the diameter of the wire rope. To choose the correct number of clamps for the second combined technique we tested assemblies with 3 clamps (1 ferrule and 2 clips, as in Figure 51a) and assemblies with 2 clamps (2 clips, as in Figure 51b), finding the latter more performing for a 3 mm single strand zinc-coated wire rope.

The Flemish eyes of the second combined technique pass through the threaded eyebolts of a turnbuckle (Figure 51a). By rotating the metal frame of the eye-eye turnbuckle, it is possible to screw both eyebolts in or out simultaneously – without twisting the eyebolts or attached ropes – thus adjusting the tension of the loop-shaped ropes.

Peer-reviewed version available at *Materials* **2019**, *12*, 1171; doi:10.3390/ma12071171

The clamping system of the second combined technique is longer than it is for the first combined technique. Nevertheless, it is possible to contain the second clamping system in the thickness of the wall specimens (Figure 52).

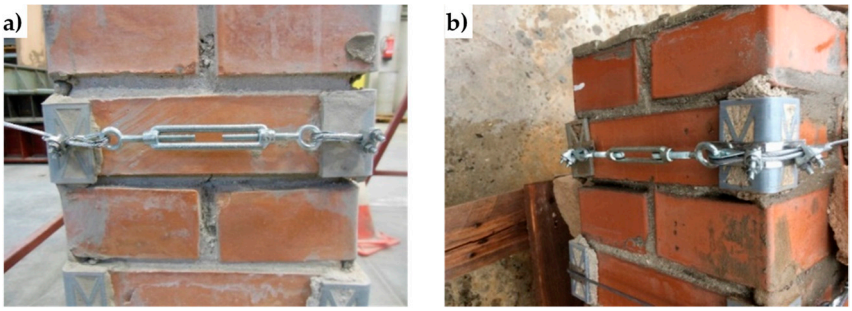

Figure 52. a) Detail of the placement of the clamping system along the thickness of the brick wall (23 cm); b) Detail of the placement of the two clips at the corner of the brick wall.

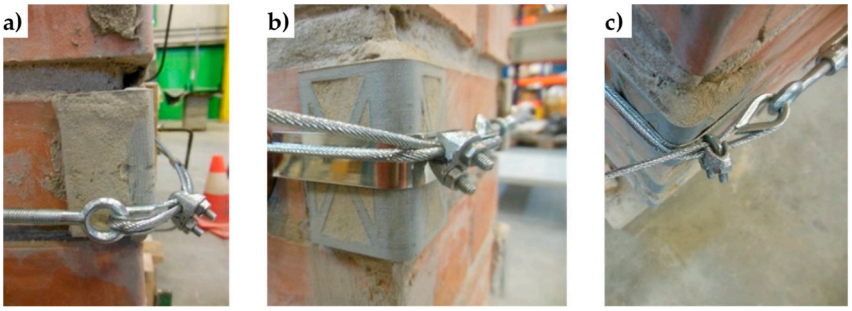

Figure 53. a) Indentation marks on a rounded angle after pre-tensioning and removal of the tying system, in the absence of a protective element between the steel wire rope and the PLA element; b) How a piece of steel ribbon protects a PLA rounded angle: front view; c) How a piece of steel ribbon protects a PLA rounded angle: top view.

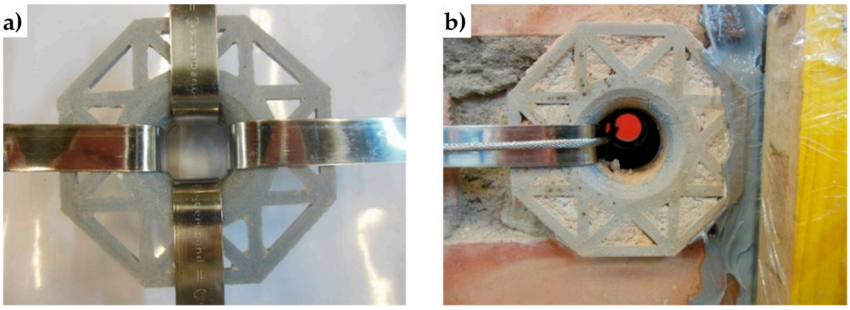

Figure 54. a) Arrangement of 4 pieces of steel ribbons to protect the rounded corners of the PLA funnel plates; b) Installation of a steel wire rope on a piece of steel ribbon, protecting the rounded corner of a PLA funnel plates.

To protect the rounded corners of the 3D printed elements, the second combined technique also uses some small pieces of steel ribbons, inserted between the steel wire ropes and the PLA elements (Figure 52b, Figure 53b,c and Figure 54). In fact, in the absence of the pieces of steel ribbons, the pre-tensioning causes the steel wire ropes to indent the rounded corners of the 3D printed elements, as shown in Figure 53a.

The arrangement of the steel wire ropes to tie the CFRP strips together by the second combined technique follows the general pattern shown in Figure 55, where the eye-eye turnbuckles clamp the steel wire ropes partly on the front side, partly on the rear side and, partly, on the lateral sides. As with the first combined technique, the transverse ties pass over the CFRP strips and under the longitudinal ties.

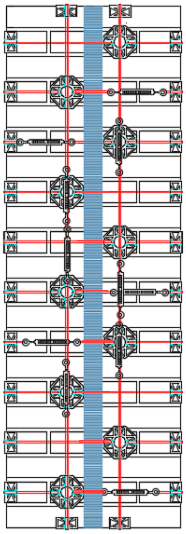

Figure 55. Scheme of the arrangement of the steel wire ropes in the second combined technique.

6. Conclusions

In the present paper, we deepened the out-of-plane behavior of the retrofitting system introduced in [16], consisting of a mechanical coupling between steel straps and CFRP strips. In particular, we have clarified how the transfer of stresses from the steel straps to the CFRP strips delays delamination on both sides of a bent beam, allowing us to exploit the strengthening properties of the CFRP strips better.

Since the retrofitting system develops in the thickness of the masonry wall, it is useful to provide a bracing effect against the hammering action of floors. Actually, compared to other bracing systems the straps/strips technique is more appealing for more than one reason:

- It is minimally invasive;
- The three-dimensional net of straps provides the building with a box-type behavior;
- Retrofitting does not excessively increase the total mass of the building, thus limiting the attraction of seismic forces;
- Once the masonry wall has cracked, the straps have exhausted their strengthening function but find a second use, starting to work as a device of safeguarding life.

Our theoretical analysis suggested us to test the flexural strength of masonry walls reinforced with the straps/strips technique, modifying the number of straps per loop. The experimental results showed us that the failure mechanism of the masonry walls with CFRP strips changed from brittle to ductile when also the steel straps were applied. In particular, the two staggered nets of steel straps provided ductility to the crack propagation in Mode I, along the mortar bed joints. This allowed the formation of several plastic hinges without ever reaching the collapse of the specimens.

Furthermore, we noted that the longitudinal and transverse straps contribute in different ways to the mechanical behavior of the specimens, as the transverse straps exploit the ribbon stiffness and the friction forces at the interface to increase the delamination load, while the longitudinal straps take advantage of strength and ductility to improve the post-delamination behavior.

Noting that the transverse straps are all the more effective as higher their stiffness suggested us to replace the steel straps with steel wire ropes, to improve the expected result of this experimental program, that is, increasing the out-of-plane strength of masonry walls.

The results of the straps/strips technique with steel wire ropes are currently under evaluation. What we can expect now is that the best choice to meet both needs of increasing the out-of-plane strength and safeguarding life is to use steel wire ropes for the transverse straps and steel ribbons for the longitudinal straps. In fact, highly pre-tensioned steel wire ropes will provide the wall with a bracing effect by counteracting the delamination of the CFRP strips and slightly pre-tensioned steel

ribbons will act as dampers by allowing the formation of numerous dissipative plastic hinges, also avoiding the structural collapse.

Funding: This research received no external funding.

Acknowledgments: The results presented here are part of the CIMEST Scientific Research on the Identification of Materials and Structures, DICAM, Alma Mater Studiorum, Bologna (Italy). The authors are grateful to Emanuele Minelli for his active collaboration in the experimental program.

Conflicts of Interest: The authors declare no conflict of interest.

References

1. Akhoundi, F.; Vasconcelos, G.; Lourenço, P.B. Experimental Out-Of-Plane Behavior of Brick Masonry Infilled Frames. *Int. J. Archit. Herit.* in press.
2. Csikai, B.; Ramos, L.F.; Basto, P.; Moreira, S.; Lourenço, P.B. Flexural out-of-plane retrofitting technique for masonry walls in historical constructions. Proceedings of SAHC2014 – 9th International Conference on Structural Analysis of Historical Constructions, Mexico City, Mexico, 14–17 October 2014; Meli, R., Peña, F., Chávez, M., Eds.; 2014.
3. Lourenço, P.B. Technologies for Seismic Retrofitting and Strengthening of Earthen and Masonry Structures: Assessment and Application. In *Recent Advances in Earthquake Engineering in Europe, ECEE 2018, Geotechnical, Geological and Earthquake Engineering*, Pitilakis K. (eds), Springer, Cham, 2018; Volume 46, 501–518.
4. Corradi, M.; Di Schino, A.; Borri, A.; Rufini, R. A review of the use of stainless steel for masonry repair and reinforcement. *Constr. Build. Mater.* **2018**, *181*, 335–346.
5. Ferretti, E.; Pascale, G. Some of the Latest Active Strengthening Techniques for Masonry Buildings: A Critical Analysis. *Materials* under review.
6. Cilia, M.; Cipolla, I.; Colajanni, P.; Marnetto, R.; Recupero, A.; Spinella, N. Prove sperimentali su travi in c.a. rinforzate con metodo CAM®: valutazione del comportamento a taglio. *Progettazione sismica* **2015**, *VII*(3), 93–108.
7. Dolce, M.; Nigro, D.; Ponzo, F.C.; Marnetto, R. The CAM system for the retrofit of masonry structures. Proceedings of 7th International Seminar on Seismic Isolation, Passive Energy Dissipation and Active Control of Vibrations of Structures, Assisi, Italy, 2-5 October 2001, 2001.
8. Dolce, M.; Ponzo, F.C.; Di Croce, M.; Moroni, C.; Giordano, F.; Nigro, D.; Marnetto, R. Experimental assessment of the CAM and DIS-CAM systems for the seismic upgrading of monumental masonry buildings. Proceedings of PROHITECH 09 - 1st International Conference on Protection of Historical Constructions, Rome, Italy, 21-24 June 2009, Publisher: CRC Press/Balkema, Leiden, the Netherlands, 2009; 1021–1028.
9. Dolce, M.; Ponzo, F.C.; Goretti, A.; Moroni, C.; Giordano, F.; De Canio, G.; Marnetto, R. 3d dynamic tests on 2/3 scale masonry buildings retrofitted with different systems. Proceedings of The 14th World Conference on Earthquake Engineering, Beijing, China, 12-17 October 2008.
10. Leonori, M.; Vari, A. L'influenza della tipologia di terreno sui meccanismi locali di collasso degli edifici in muratura e miglioramento sismico con il sistema CAM®. In Dynamic Interaction of Soil and Structure (DISS_15), Proceedings of The 4th International Workshop on Archaeology, Cryptoportici, Hypogea, Geology, Geotechnics, Geophysics, Rome, Italy, 12-13 November 2015; Monti, G., Valente, G., Eds.; Università dell'Aquila, Dipartimento DICEAA – Sapienza, Università di Roma, Italy, 2015; 1–15.
11. Marnetto, R. Sviluppo ed applicazioni delle tecniche antisismiche presso la società TIS SpA di Roma. Proceedings of Seminario di studi sui sistemi e tecnologie antisismici, Rome, CNR, Italy, 12 September 2007; 2–27.
12. Marnetto, R.; Vari, A. Linee Guida – Cuciture attive per la muratura: procedura generale per la progettazione, modellazione, calcolo e verifica di edifici in muratura rinforzati con il sistema di cucitura attiva CAM; EDIL CAM Sistemi S.r.l.: Roma, Italy, October 2015.
13. Marnetto, R.; Vari, A.; Marnetto, L.; Leonori, M. Conservare l'edilizia in muratura: il sistema CAM – Cuciture attive dei manufatti; Edizioni PREprogetti: Roma, Italy, 2014.
14. Ferretti, E. Effectiveness of Active Confinement Techniques with Steel Ribbons: Masonry Buildings. *European Journal of Engineering and Formal* Sciences **2018**, *2*(3), 17–29.

15. Ferretti, E.; Casadio, E.; Di Leo, A. Masonry Walls under Shear Test: a CM Modeling. *CMES-Comp. Model. Eng.* **2008**, *30*(3), 163–189.
16. Ferretti, E. Attaining a Beam-Like Behavior with FRP Strips and CAM Ribbons. *European Journal of Engineering and Formal* Sciences **2018**, *2*(3), 6–16.